Energy & Environmental Science

RSC Publishing

PAPER

View Article Online
View Journal | View Issue

Cite this: *Energy Environ. Sci.*, 2013, **6**, 2203

Optimization of polymer photovoltaic cells with bulk heterojunction layers hundreds of nanometers thick: modifying the morphology and cathode interface†

Hui Joon Park,‡[a] Hyunsoo Kim,[b] Jae Yong Lee,[b] Taehwa Lee[c] and L. Jay Guo*[abc]

In polymer photovoltaic (PV) cell, it is desirable to use a relatively thick polymer semiconductor film in order to maximize the light absorption, and to achieve better controllability and reproducibility of the film in manufacturing processes. However, the low fill factor due to restricted charge transport and extraction at large film thickness serially limits the performance of the polymer PV cell. In this work, we investigate the factors that can impact the device performances as film thickness is increased. We also introduce ways to help alleviate these problems in thick BHJ PVs. Our measurement results, based on the space-charge limited-current (SCLC) model and the photo-induced carrier extraction by linearly increasing voltage (photo-CELIV) method, show that the thicker BHJ devices have relatively low electron mobility compared with hole mobility, which directly correlates with high contact resistance at the top cathode interface that prevents efficient transport of photo-generated electrons. Specifically, we found that the newly introduced ESSENCIAL fabrication process helps improve the blend donor and acceptor domain morphologies; and adding an ultrathin C_{60} layer at the cathode interface helps improve the surface morphology and significantly reduce the contact resistance. The effects of the added thin C_{60} layer on PV cells were further studied by examining several important diode characteristics. Our results proved that this layer not only decreases the contact resistance at the cathode but also improves the hole-blocking, thereby providing significantly suppressed recombination at the cathode interface. Consequently, the fabricated PV devices optimized in morphology and interface show significantly improved internal quantum efficiency (IQE) as compared with the thermally annealed conventional PV cells, leading to 5.11% PCE from a P3HT:PCBM blend system. The modifications to the fabrication of BHJ PV cells described in this work allow for photoactive layers to be hundreds of nanometers thick for efficient light absorption and better controllability.

Received 18th December 2012
Accepted 8th May 2013

DOI: 10.1039/c3ee24410e

www.rsc.org/ees

Broader context

Bulk heterojunction (BHJ) polymer PV cell is a promising candidate as a future renewable energy source due to their low cost, easy processability and applicability to flexible substrates. To improve their light absorption property for better energy conversion and the film controllability in manufacturing processes, relatively thick polymer semiconductor film is highly desirable. In this work, we investigate the factors that affect their performances as the film thickness is increased, and it is found that the BHJ morphology and the interfacial property can be optimized by a new fabrication method and an additional buffer layer, respectively. Consequently, the modifications to the fabrication of BHJ PV cell described here allow for photoactive layer to be hundreds of nanometers thick and enhance device performances.

I Introduction

Polymer photovoltaic (PV) cells are promising candidates as a future renewable energy source due to their low cost, easy processability and acceptable energy conversion performance when applied to flexible substrates.[1–8] Especially, bulk heterojunction (BHJ) polymer PV cell, which consists of interpenetrating nanoscale networks of electron-donor and electron-acceptor, has phase-separated domain sizes on the order of the exciton diffusion length, which allows for efficient exciton dissocation.[8–12] Because of this, BHJ PV cell is widely accepted as

[a]*Macromolecular Science & Engineering, The University of Michigan, Ann Arbor, MI, 48109, USA. E-mail: guo@umich.edu; Fax: +1-734-763-9324; Tel: +1-734-647-7718*
[b]*Electrical Engineering & Computer Science, The University of Michigan, Ann Arbor, MI, 48109, USA*
[c]*Mechanical Engineering, The University of Michigan, Ann Arbor, MI, 48109, USA*

† Electronic supplementary information (ESI) available. See DOI: 10.1039/c3ee24410e

‡ Present address: Portland Technology Development, Logic Technology Development, Intel Corporation, Hillsboro, OR 97124, USA.

effective in achieving high efficiency using polymer materials. The power conversion efficiencies (PCEs) of single BHJ PV cells have steadily increased and now reached up to 7–8%,[13,14] and very recently to close to 12% and those from the most commonly used poly(3-hexylthiophene):[6,6]-phenyl C_{61} butyric acid methyl ester (P3HT:PCBM) blend system are 3–5%.[15]

One of the primary requisites to achieve high power conversion efficiency (PCE) from BHJ PV cell is to maximize light absorption for efficient exciton generation. For a conventional film with a given absorption coefficient, absorption can be simply improved by increasing the film thickness.[16] Moreover, the increased film thickness minimizes the additional absorption loss in a multilayer structure induced by optical interference effects. Also a thicker film can facilitate the practical fabrication of the polymer PVs by a roll-to-roll process, and guarantees reproducibility in manufacturing. However, the random nature of the nanodomains in a BHJ structure makes the optimization process challenging as the thickness of the photoactive layer is increased. This is particularly evident in the vertical non-uniformity of blend components, especially in the commonly used P3HT:PCBM blend system.[17–20] In this system, the electron-donor phase dominates the active layer near the top cathode because of the difference in surface energies of the donor and acceptor components, and this distribution becomes more prominent in a thicker layer. Such a configuration is opposite of the ideal PV cell structure, which requires a donor-rich phase near the anode and an acceptor-rich phase near the cathode, and results in unfavorable charge transport to the electrodes. Therefore, the improvement of BHJ PV cell performance is not always guaranteed by increasing the thickness of the photoactive layer for the purpose of improved light absorption and exciton generation.[21–23]

To date, various film formation techniques by spin-casting, blade coating or spray coating, followed by additional treatment such as thermal and solvent annealing, have shown significant success in optimization of complex nanostructures in BHJ layers.[24–29] However, most of these works have primarily focused on thin photoactive layers around a hundred nanometers thick because of the aforementioned difficulty of optimizing thicker BHJ devices. Furthermore, the non-uniformity of components in the vertical direction cannot be solved by conventional film-casting techniques alone. Recently we reported that much more uniform vertical distributions can be achieved by casting the blend solution using a new ESSENCIAL process, which allows Evaporation of Solvent through Surface ENCapsulation and with Induced ALignment of polymer chains by applied pressure.[12] Excellent results were obtained due to the improved vertical arrangement of the donor and acceptor phases.

The focus of this work is to improve the performance of BHJ OPV cells having hundreds of nanometers thick photoactive layers. Such thick devices usually suffer from low fill factors due to restricted charge transport and extraction. For this reason, the charge transport properties, which are closely related to blend morphology, are first investigated using single-carrier devices. In addition, surface morphology, which affects the interfacial properties between the blend layer and electrode, is further studied by evaluating the contact resistances at the electrode. Our measurement results, based on the space-charge limited-current (SCLC) model and the photo-induced carrier extraction by linearly increasing voltage (photo-CELIV) method, show relatively lower electron mobility than the hole mobility in thicker BHJ devices, which correlates with the high contact resistance measured at the top cathode interface that prevents efficient transportation of photo-generated electrons. These issues can be resolved by controlling blend morphologies with the ESSENCIAL process, of which application has been limited to ~200 nm until now, as well as by improving the surface morphology with an additional ultrathin C_{60} layer at the cathode interface. The effects of an additional C_{60} layer on the PV cells are examined by diode characteristics such as series resistance, shunt resistance and the diode ideality factor. Our results prove that this layer is beneficial not only for decreasing the contact resistance at the cathode but also for improving the hole-blocking property. Furthermore, these findings are further verified by the simulation results, which show significantly suppressed surface recombination with the additional layer. The resulting optimized PV cell has a BHJ active layer 380 nm thick with high short-circuit current and high fill factor, leading to 5.11% PCE from a P3HT:PCBM blend system, and provides maximum 30% improvement (not ratio) in the internal quantum efficiency (IQE) as compared with conventional BHJ PV cells.

II Result and discussion

Fig. 1 shows the short-circuit currents, fill factors, PCEs and current density (J)–voltage (V) characteristics of a series of BHJ PV cells with increasing thickness of the photoactive layer. The data presented in the left panel are for devices fabricated using the conventional thermal annealing process after spin-casting, denoted by thermal annealing hereafter. Also included are the data showing the impact of adding a thin C_{60} layer at the top of the device before depositing the cathode, which will be discussed later in this paper. Most notable for the thermally annealed samples is that PCE values begin to decrease as the thickness of the photoactive layer is increased over 300 nm (Fig. 1e), mainly because of decreased fill factors (Fig. 1c). This indicates that thermal annealing is not adequate to optimize the BHJ photoactive layer for thicker photoactive films. As discussed, we believe that the non-ideal vertical distribution of donor and acceptor components,[17–20] which is inevitably induced during the spin-casting process, is one of the important factors causing this limitation. In comparison, the right panel shows the corresponding performance characteristics of devices fabricated using the new ESSENCIAL technique. The ESSENCIAL process utilizes a gas- and solvent-permeable membrane to provide increased surface energy than the air interface in the spin-coating process, and was shown to impart a much more uniform vertical distribution of the blend components.[12] The merits of the ESSENCIAL process are not only limited to forming a favorable, vertical distribution of components, but also to providing advantageous morphological properties such as a large interfacial area for improved exciton dissociation and continuous domain pathways for efficient

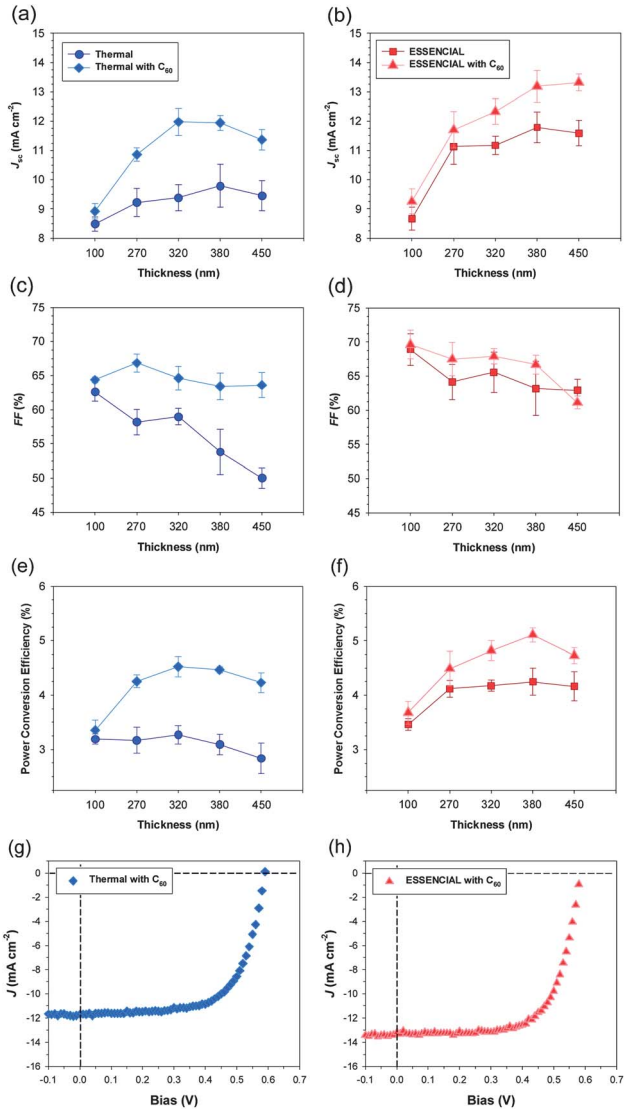

Fig. 1 Performances of P3HT:PCBM BHJ PV cells according to the photoactive layer thickness with/without C_{60} layer: short-circuit current densities of (a) thermally annealed and (b) ESSENCIAL devices, fill factors of (c) thermally annealed and (d) ESSENCIAL devices, and power conversion efficiencies of (e) thermally annealed and (f) ESSENCIAL devices; *J–V* curves of polymer PV cells: (g) thermally annealed device (320 nm active layer with C_{60}, $J_{sc} = 11.97$ mA cm^{-2}, $V_{oc} = 0.58$ V, FF = 64.6%, PCE = 4.52%) and (h) ESSENCIAL device (380 nm active layer with C_{60}, $J_{sc} = 13.19$ mA cm^{-2}, $V_{oc} = 0.58$ V, FF = 66.7%, PCE = 5.11%): circle, diamond, square and triangle represent thermal anneal without C_{60}, thermal anneal with C_{60}, ESSENCIAL without C_{60} and ESSENCIAL with C_{60}. All data were measured at AM 1.5 G (100 mW cm^{-2} intensity).

charge transportation.[12] Detailed information about improved morphology such as atomic force microscopy (AFM), photoluminescence (PL) and X-ray photoelectron spectroscopy (XPS) can be found elsewhere, and will not be repeated here.[12] Thus, all the performance metrics of PV cells fabricated by the ESSENCIAL process shown on the right panel in Fig. 1 exceed those of thermally annealed devices. The vertical uniformity from the ESSENCIAL process is generated by using a gas-permeable film that provides a higher surface energy than air, thereby preventing the P3HT component, which has a lower surface energy, from migrating to the top air intersurface. Since the surface energy effects mostly originate from the change of components at the surface of the photoactive layer, it is expected that they become less effective as the thickness of active layer is increased. This is the reason PCEs cannot continuously improve by simply increasing the thickness (Fig. 1f). Nonetheless, it is noteworthy that a high fill factor value greater than 0.6 is maintained even in 450 nm-thick ESSENCIAL devices (Fig. 1d). We believe there is still room to further improve the PCE values if we can determine the remaining issues with the blend morphology in these thicker photoactive layers.

In order to further understand the performance of the PV cells, we first examine the charge transportation properties closely associated with the morphology by measuring the charge carrier mobilities using electron-only and hole-only devices. The hole-only device was fabricated by replacing lithium fluoride (LiF) with high work-function molybdenum oxide (MoO_3) to block the injection of electrons from the Al cathode. The electron-only device was prepared by changing PEDOT:PSS to low work-function cesium carbonate (Cs_2CO_3) to block the injection of holes from the ITO anode.[30] In this work, both hole- and electron-mobility are calculated using two different methods. The first approach is fitting the dark *J–V* curves of single-carrier devices at low voltage to the SCLC model. The current density in this model is represented by $J = 9\varepsilon_o\varepsilon_r\mu V^2/8L^3$, where $\varepsilon_o\varepsilon_r$ is the permittivity of the component, μ is the carrier mobility, and L is the thickness.[31] The second approach is the photo-CELIV method, which is often used to calculate the carrier mobility and recombination behavior in low conductivity materials.[32] When a reverse, sawtooth-shaped bias is applied with an increasing rate A (V s^{-1}) in the dark to low conductivity materials such as polymer PV cells, a rectangular-shaped current transient having a constant value is measured as an electrical signal. This constant current value is a capacitive displacement current $j(0)$ (C s^{-1}). In this condition, when the device is exposed to pulsed laser excitation, photocharges are generated in the photoactive layer, and they either recombine or are extracted by the electric field. By measuring t_{max}, which occurs at the maximum photocurrent, and comparing the ratio of extracted current (Δj) to constant current ($j(0)$), we can calculate the mobility of carriers using eqn (1).[32]

$$\mu = \frac{2d^2}{3At_{max}^2\left(1 + 0.36\,\frac{\Delta j}{j(0)}\right)} \quad (\Delta j \le j(0)) \qquad (1)$$

where d is the thickness of the photoactive layer. As shown in Table 1, the electron mobility in the thermally annealed device (1.23×10^{-4} cm^2 V^{-1} s^{-1}), calculated by the SCLC model, is about a third of the hole mobility (3.27×10^{-4} cm^2 V^{-1} s^{-1}). Even in ESSENCIAL device, the electron mobility (5.25×10^{-4} cm^2 V^{-1} s^{-1}) is approximately half of the hole mobility (11.50×10^{-4} cm^2 V^{-1} s^{-1}). Photo-CELIV results also show a similar trend of significantly lower electron mobility than hole mobility, and the reduction calculated by this method is much larger than that by SCLC. The validity of the hole mobility values obtained by photo-CELIV will be discussed with the mobility results of single-carrier devices with an additional C_{60} layer.

Table 1 Effect of the additional C_{60} layer on the carrier mobilities and diode characteristics of BHJ PV cells fabricated by thermal annealing and ESSENCIAL processes. The carrier mobilities are calculated using the SCLC model and photo-CELIV method. The thickness conditions showing the highest devices performances (320 and 380 nm for thermal annealing and ESSENCIAL, respectively) are selected for measurement. The values in brackets may have significant experimental uncertainty. All of the carrier mobilities measured from the devices are effective mobilities, as explained in the text

		Carrier mobility [10^{-4} cm^2 V^{-1} s^{-1}]				Diode characteristics					
		Hole [μ_h]		Electron [μ_e]		Shunt resistance (Ω cm^2)		Series resistance (Ω cm^2)		Diode ideality factor	
Method	Tool	No C_{60}	With C_{60}	No C_{60}	With C_{60}	No C_{60}	With C_{60}	No C_{60}	With C_{60}	No C_{60}	With C_{60}
Thermal	SCLC	3.27	3.35	1.23	5.84	4.20×10^2	1.64×10^3	10.5	6.4	1.94	1.95
	CELIV	(2.22)	(1.95)	0.27	1.32						
ESSENCIAL	SCLC	11.50	10.90	5.25	13.60	4.28×10^3	1.65×10^4	7.3	5.3	1.87	1.80
	CELIV	(4.66)	(3.56)	0.90	2.10						

We speculate that the unbalanced mobility obtained from the devices having BHJ layers hundreds of nanometers thick is an indication that the electron collection at the cathode is not as efficient as the collection of holes at the anode. It was also previously shown by other researchers that P3HT tends to segregate to the top surface during spin-coating.[17–20] We conjecture that a fairly large amount of donor material is accumulated at the top surface in the thick BHJ device and thereby hampering the transport of photoelectrons at the cathode. This trend is more discernible in the spin-coated and thermally annealed BHJ layer. Here, we suggest inserting an additional thin acceptor layer (~5 nm C_{60}) between the photoactive layer and the cathode as a possible solution to this congestion problem. The results are outstanding, for both thermally annealed sample and the ESSENTIAL sample as shown in Fig. 1. We further investigate the effect of an additional thin C_{60} layer by evaluated contact resistances at the cathode interface to gain better understanding the effect of the added thin C_{60} layer. As shown in Fig. 2a, organic thin film transistor (OTFT)-like devices were used for the measurement of resistance,[33,34] and a bottom PEDOT:PSS layer was inserted to provide the same surface condition for coating the BHJ photoactive layer. The measured resistances, which are similar to values that can be obtained from the linear regime of OTFT output characteristics, are represented by $V/I = R = 2R_c + R_{\square}L/W$, where V is bias, I is current, R is the total resistance, R_c is contact resistance, and $R_{\square}$ is sheet resistance. L is the distance between LiF/Al electrodes and W is the constant electrode width. The measured resistances are plotted by the distances between the electrodes, which have a fixed width, and the contact resistance is taken by the y-intercept of the resistance axis. For both ESSENCIAL and thermally annealed devices, the contact resistances by adding a thin C_{60} layer are significantly reduced as compared with the ones without the C_{60} layer, as summarized in Fig. 2b. Another remarkable feature from these results is that the contact resistances in the ESSENCIAL devices (150–1000 kΩ) are over two orders of magnitude smaller than those in thermally annealed devices (30–250 MΩ). In order to identify the reason, we measured the contact resistances of a PCBM (*i.e.* C_{60}-derivative) single layer and a P3HT single layer with LiF/Al electrodes. As shown in Fig. 2b, the resistances between PCBM and the cathode show a similar magnitude and range of values with those in ESSENCIAL devices. They are much smaller than those between P3HT and the cathode, which show a similar magnitude and range of values with those in thermally annealed devices. Therefore, we can confirm that much larger

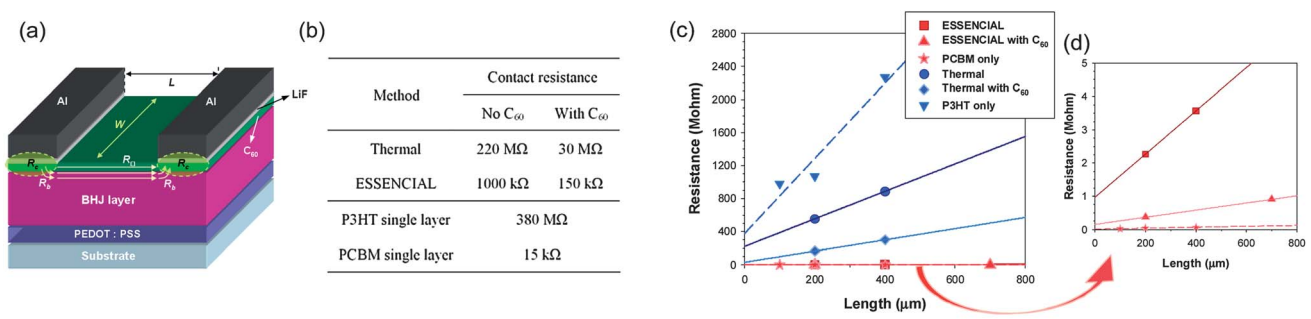

Fig. 2 (a) The device architecture for contact resistance measurements. A PEDOT:PSS layer was used to provide the same surface condition as the PV cell. R_c is contact resistance, R_b is bulk resistance, and $R_{\square}$ is sheet resistance. L is the distance between Li/Al electrodes and W is their constant width. (b) Summary of the calculated contact resistances. (c) Measured resistances according to the distance between LiF/Al electrodes. The y-axis intercepts are contact resistances, R_c and the slopes are sheet resistances, $R_{\square}$: square, triangle, star, circle, diamond and inverse triangle represent ESSENCIAL without C_{60}, ESSENCIAL with C_{60}, PCBM single layer, thermal anneal without C_{60}, thermal annealed device with C_{60}, P3HT single layer, respectively. The thickness conditions of the BHJ layers are the same as in Table 1 and the area of electrode is 0.08 cm^2.

P3HT domains are assembled at the top surface of the thermally annealed photoactive layer than the ESSENCIAL photoactive layer, and these domains induce much worse electron transport at the cathode interface, resulting in lower PCE values. In contrast, the relatively large amount of PCBM at the surface of ESSENCIAL devices, which comes from better vertical uniformity as confirmed from our previous study,[12] forms better contact between the photoactive layer and electrode and provides better electron transportation to the electrode. This also means we need to re-consider the mobility values discussed before, as the carrier mobility is an intrinsic property of the material, which can be affected by the donor–acceptor morphology in the bulk PV film, but not by the contact interface. However in the experiment, the voltage drop at the contact would affect the obtained mobility values. For this reason, we will call the mobility calculated from the devices here as effective mobility, which is affected by the contact interface. It can be used to compare the relative effectiveness of carrier extraction at the electrode contact with buffer layer such as C_{60} in this work. All the calculated carrier mobilities with and without an additional C_{60} layer, characterized by both SCLC and photo-CELIV, are summarized in Table 1. The decreased contact resistance originating from the additional C_{60} layer indeed results in increased effective mobility of the electron. However, the effective mobility of hole remains almost the same after inserting the C_{60} layer. This result is expected as transport of holes is not directly related to the cathode interface. These show evidence that the positive effect of a C_{60} layer is from the improved electron transport at the cathode interface. The detailed photo-CELIV transients used for determining electron and hole mobility are shown in Fig. 3a/c and b/d, respectively,

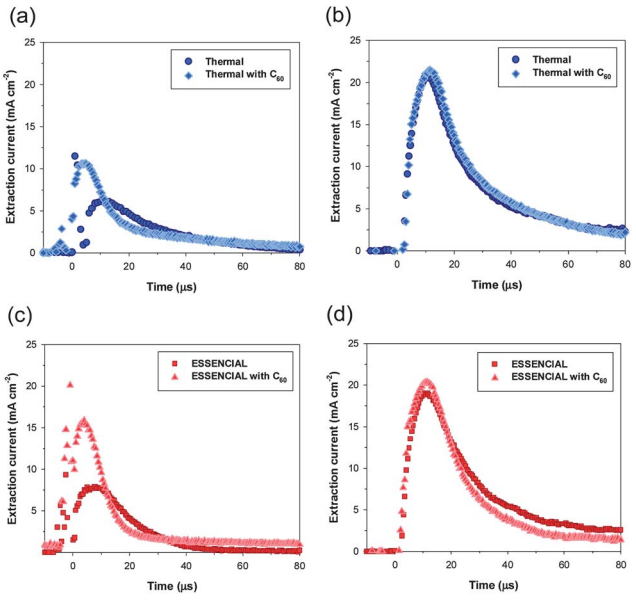

Fig. 3 Photo-CELIV transients of single-carrier devices fabricated by thermal annealing and ESSENCIAL with and without C_{60} layer; the symbols are the same in Fig. 1: (a) electron-only devices by thermal annealing; (b) hole-only devices by thermal annealing; (c) electron-only devices by ESSENCIAL; (d) hole-only devices by ESSENCIAL. The thickness conditions of the BHJ layers are the same as in Table 1.

and the dark *J*–*V* curves at low voltage for the SCLC model are shown in Fig. S1.† During our measurements, the photo-CELIV signals of hole-only devices did not show complete capacitive displacement current and the measured Δj was also larger than $j(0)$, which did not satisfy the conditions for eqn (1). However, the trend of hole mobility matches with that obtained by SCLC model, and the possible deviation from actual values do not affect any conclusion in this work.

Another potential deviation from our mobility results obtained by photo-CELIV is the charge accumulation issue in single-carrier devices. The unbalanced charge transport usually induces charge carrier accumulation near contact, changing the electric field within photoactive layer and consequently the charge extraction.[35] In the electron-only and hole-only devices, the unbalanced charge transport, originating from the blocking layer, may affect the extraction of opposite carriers, and accordingly influences the measured mobility, because the CELIV measurement is based on determining the charge extraction depth.[36,37] It is also worth noting that the light intensity in typical photo-CELIV measurement is many orders of magnitude higher than the conventional PV cell performance test conditions (*e.g.* 100 mW cm^{-2} intensity for *J*–*V* curves). Therefore, one should consider the validity of the mobility obtained by this method in a PV cell structure. Mozer *et al.* showed that the extraction current saturated at light intensities above 1 μJ cm^{-2} per pulse in their BHJ PV cells,[38] and this light intensity independent recombination kinetics in the μs regime, related to thermally activated charge carrier recombination,[39] has been reported by transient absorption measurements.[40] Under 1 μJ cm^{-2} per pulse intensity, t_{max} remained almost constant showing that the mobility in these charge carrier concentrations was not variable. Another factor that has more important effect is the forward bias applied during the light pulse in photo-CELIV, where charges in the device structure are both injected from the contact and by photo-generation. Therefore, the time to extract them is longer than what is required to extract only the photo-generated carriers, and the calculated mobility can be underestimated. A modified CELIV technique, called open circuit corrected charge carrier extraction (OTRACE), can be used to measure the mobility under PV cell operating conditions by correcting both light intensity and underestimation issues.[41] Even though this effect may be able to induce the experimental errors on our measured values, it is evident that the effective electron mobilities from the devices with the additional C_{60} layer are increased compared with those from the devices without C_{60} layer. Meanwhile, overall the mobilities of both hole and electron in ESSENCIAL devices are higher than those in thermally annealed devices, indicating that a much more favorable morphology can be achieved using the ESSENCIAL process.

The effect of the additional C_{60} layer is further analyzed from a diode point of view. The diode characteristics of BHJ polymer PV cells have often been described by the generalized Shockley equation (eqn (2)).[42,43]

$$J = \frac{R_{sh}}{R_s + R_{sh}}\left\{J_s\left[\exp\left(\frac{q(V - JR_s)}{nkT}\right) - 1\right] + \frac{V}{R_{sh}}\right\} - J_{ph}(V) \quad (2)$$

In this equation, R_{sh} is the shunt resistance, R_s is the series resistance, J_s is the dark saturation current density, n is the diode ideality factor, and $J_{ph}(V)$ is the voltage-dependent photo-generated current density. All these parameters can be obtained by fitting the J–V curves with eqn (2) (shown in Fig. S2 in ESI†), and the results are summarized in Table 1. The major change that comes with an added C_{60} layer is the increase in shunt resistances in both ESSENCIAL (4.28×10^3 to 1.65×10^4 Ω cm^2) and thermally annealed (4.20×10^2 to 1.64×10^3 Ω cm^2) devices. This result can be explained by the suppressed hole leakage current at the cathode because the added C_{60} layer prevents donor domains at the top surface of the device from directly contacting the cathode and functions as an effective hole-blocking layer. The highest occupied molecular orbital (HOMO) energy level of C_{60} is lower than that of the donor which effectively acts as a barrier to holes. Meanwhile, the diode ideality factors, which reflect the properties of the interface between donor and acceptor,[44,45] are almost unchanged with the addition of C_{60}. This effect is expected as the additional thin C_{60} layer should not have any effect on the internal BHJ morphology.

The facilitated electron extraction to the cathode and hole-blocking by the addition of a thin C_{60} layer should also lead to reduced recombination at the interface. We performed the simulations by solving the continuity equations and Poisson's equation.[46] The distribution of donor and acceptor semiconductors is assumed to be uniform in the vertical direction. The exciton generation from the light absorption is calculated using transfer matrix formulation to consider the interference effect of multiple thin layers,[47] and the selective contact approach is utilized to investigate the effect of C_{60} layer at the interface.[48] J_{sc} calculated by the simulation shows the increasing trend with the oscillatory nature that comes from the optical interference effect, as the blend thickness is increased (Fig. 4a). The additional C_{60}, which is considered to improve the electron transport and hole-blocking at the cathode interface, significantly suppresses the recombination at the interface (Fig. 4b), leading to the improved J_{sc} (Fig. 4a). This enhancement of J_{sc} is more prominent in the thicker samples because the built-in potential decreases with thickness, and the surface recombination represents an even more significant charge loss mechanism in the thicker devices. The enhancement shows the discrepancy between experimental and simulation results around 400 nm thickness ranges. We believe this is due to the fact that in the actual samples, the P3HT rich region near the cathode interface becomes more prominent with increased layer thickness, but such thickness-dependence is not taken into account in our current model.

Finally, the optimized morphology and interfacial property also provide high internal quantum efficiency (IQE), which means a higher percentage of the photo-generated excitons is fully dissociated and transported to the electrode without recombination (Fig. 4c). To calculate IQE accurately, the absorption efficiency was obtained by eliminating the parasitic absorption in PV devices, calculated by transfer matrix method, from the reflection spectrum.[49] The external quantum efficiency (EQE) was experimentally measured. These plots are shown in Fig. S3 in the ESI.† As shown in Fig. 4c, the optimized PV cell based on the ESSENCIAL process and with an additional C_{60} layer shows the highest IQE, which is maximally about 30% higher than that of the thermally annealed conventional PV cell (from 61% to 90% at 580 nm). That PV cell shows both high photocurrent (13.19 mA cm^{-2}) and fill factor (66.7%), giving high power conversion efficiency of 5.11% in a BHJ blend film of 380 nm thick. All the device performances are summarized in Fig. 1.

III Conclusion

Thick BHJ devices show low fill factors and decreased PCEs as compared to thin BHJ devices. We have investigated factors, which have negative effects on the device performances, particularly as the film thickness is increased. Through this study, we identified several ways to help alleviate these problems. We found that the ESSENCIAL process offered more control of the blend morphology over conventional processing methods, and a C_{60}-modified interface between the blend and cathode led to more balanced charge transportation. Our results showed that the additional C_{60} layer not only significantly decreased the contact resistance, but also improved hole blocking at the cathode, suppressing recombination at the

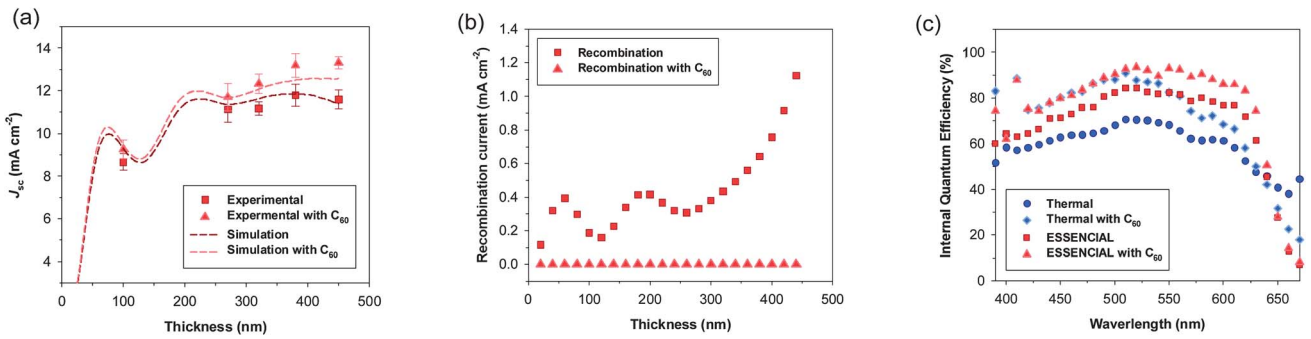

Fig. 4 (a) Short-circuit current density according to the photoactive layer thickness: symbols and dashed lines represent experimental and simulation results, respectively. The experimental results come from PV cells fabricated by ESSENCIAL process. (b) Recombination current at the cathode interface according to the photoactive layer thickness, calculated by simulation. (c) Internal quantum efficiency (IQE) of the PV cells depending on the fabrication methods. PV cells that show the highest performance were selected for comparison; the thicknesses of photoactive layers of ESSENCIAL and thermally annealed devices are 380 and 320 nm, respectively.

interface. The modifications to the fabrication of BHJ PV cell described in this work allow for photoactive layer to be hundreds of nanometers thick and enhance device performances. We anticipate that this approach can directly benefit the practical fabrication of large area polymer PV cells.

IV Experimental

A Polymer PV cells fabrication and device performance measurements

Polymer PV cells have the following configuration: transparent substrate/ITO/PEDOT:PSS/P3HT:PCBM/LiF/Al. The thermally annealed devices were fabricated by spin-casting the blend solution (dissolved in dichlorobenzene) onto a PEDOT:PSS-coated ITO substrate and subsequently annealing at 130 °C for 20 min. The ESSENCIAL process was performed by pressing the blend solution (dissolved in dichlorobenzene) onto the PEDOT:PSS-coated ITO substrate using a modified PDMS silicone film, which is gas-permeable and solvent-resistant with minimal deformation.[50] The thickness of the blend film fabricated by the ESSENCIAL method was controlled by changing the concentration of the blend solution and the applied pressure. All the film thicknesses were measured by Dektak Surface Profilometer. More details on fabrication using the ESSENCIAL method are explained elsewhere.[12] The additional C_{60} layer was thermally deposited at a pressure of 8×10^{-7} mbar before depositing the LiF (1 nm) and Al (80 nm) cathode. For hole-only devices (substrate/ITO/PEDOT:PSS/P3HT:PCBM/MoO_3/Al) 20 nm MoO_3 was deposited onto the active layer instead of LiF, and Al deposition through a shadow mask completed device fabrication. For electron-only devices (substrate/ITO/Cs_2CO_3/P3HT:PCBM/LiF/Al), 0.2 wt% Cs_2CO_3 dissolved in 2-ethoxyethanol was spin-casted on the ITO substrate at 3000 rpm and subsequently baked at 170 °C for 20 min. The remaining procedures, such as the active layer deposition and cathode deposition, were the same as in normal polymer PV cell fabrication. The device performances were measured with Keithley 2400 system by illuminating the polymer PV cells using Oriel solar simulator (equipped with Xenon lamp and AM 1.5 G filter) at the irradiation intensity of 100 mW cm^{-2}, calibrated by NREL-certified Si reference cell. The spectral mismatch of the simulated light source was corrected.[51] All the PV cell performances were measured under N_2 environment. The differences between the short-circuit current densities obtained by *J–V* curves and those calculated by EQE signal are within 5%.

B Photo-CELIV measurement

A short N_2 gas pulsed laser (337 nm, PTI GL-3300) with a 1.5 ns pulse width and a 2 J m^{-2} pulse energy was illuminated on device samples to generate charge carriers within the photoactive layers. The generated charge carriers were then extracted using a linearly increasing reverse bias pulse (sawtooth-shaped voltage pulse). The voltage pulse was created using an HP 3314A function generator. The delay time (t_{del}) between the laser flash and the triangular bias pulse was in the range of 1 to 200 μs, which was controlled by an SRS DG535 digital delay/pulse generator (Stanford Research Systems). An optical sample stage and two micro manipulators were used to establish electrical contact with the anode/cathode through which the voltage pulses (widths of $t_p = 100$ μs with a 10 kHz frequency) were applied. The peak voltage in the reverse direction was approximately $V_a = 1$–2 V and was applied to the Al cathode electrode with a varied offset bias V_{off} in the forward direction. The offset bias was set to compensate for the intrinsic built-in potential. The resulting current was monitored as a function of time using the 50 Ω input of a digital storage oscilloscope (DSO7054A, Agilent Technologies). All photo-CELIV measurements were performed at room temperature.

C Surface recombination current calculation

The surface recombination current was calculated by $S(n - n_0)$, which represented the surface recombination velocity and excessive carrier density defined by difference between charge carrier density (n) and equilibrium carrier density (n_0) at the cathode. This was applied to the boundary conditions of drift-diffusion equations to determine electrical performance.[48] The surface recombination velocity was chosen as a fitting parameter to see the effect of C_{60} as hole blocking layer. The surface recombination velocity of the devices with C_{60} layer (10^{-7} m s^{-1}) was much lower than those without C_{60} layer (10^7 m s^{-1}). This led to low surface recombination current and large short-circuit current, showing good agreement with experimental data.

Acknowledgements

This work was supported as part of Center for Solar and Thermal Energy Conversion, an Energy Frontier Research Center funded by the U.S. Department of Energy, Office of Science, Basic Energy Sciences under Award DE-SC0000957. H. J. P. acknowledges a Rackham Predoctoral fellowship from the University of Michigan.

References

1 P. Peumans, A. Yakimov and S. R. Forrest, *J. Appl. Phys.*, 2003, **93**, 3693.
2 H. Ma, H.-L. Yip, F. Huang and A. K.-Y. Jen, *Adv. Funct. Mater.*, 2010, **20**, 1371.
3 M.-G. Kang, H. J. Park, S. H. Ahn, T. Xu and L. J. Guo, *IEEE J. Sel. Top. Quantum Electron.*, 2010, **16**, 1807.
4 W. Chen, M. P. Nikiforov and S. B. Darling, *Energy Environ. Sci.*, 2012, **5**, 8045.
5 J. D. Servaites, M. A. Ratner and T. J. Marks, *Energy Environ. Sci.*, 2011, **4**, 4410.
6 B. P. Lyons, N. Clarke and C. Groves, *Energy Environ. Sci.*, 2012, **5**, 7657.
7 C. R. McNeill, *Energy Environ. Sci.*, 2012, **5**, 5653.
8 N. Espinosa, M. Hösel, D. Angmo and F. C. Krebs, *Energy Environ. Sci.*, 2012, **5**, 5117.
9 G. Yu and A. J. Heeger, *J. Appl. Phys.*, 1995, **78**, 4510.
10 G. Yu, J. Gao, J. C. Hummelen, F. Wudl and A. J. Heeger, *Science*, 1995, **270**, 1789.
11 B. Walker, A. B. Tamayo, X.-D. Dang, P. Zalar, J.-H. Seo, A. Garcia, M. Tantiwiwat and T.-Q. Nguyen, *Adv. Funct. Mater.*, 2009, **19**, 3063.

12 H. J. Park, M.-G. Kang, S. H. Ahn and L. J. Guo, *Adv. Mater.*, 2010, **22**, E247.
13 Z. He, C. Zhong, X. Huang, W.-Y. Wong, H. Wu, L. Chen, S. Su and Y. Cao, *Adv. Mater.*, 2011, **23**, 4636.
14 C. E. Small, S. Chen, J. Subbiah, C. M. Amb, S.-W. Tsang, T.-H. Lai, J. R. Reynolds and F. So, *Nat. Photonics*, 2012, **6**, 115.
15 M. T. Dang, L. Hirsch and G. Wantz, *Adv. Mater.*, 2011, **23**, 3597.
16 B. P. Rand, J. Genoe, P. Heremans and J. Poortmans, *Progr. Photovolt.: Res. Appl.*, 2007, **15**, 659.
17 M. Campoy-Quiles, T. Ferenczi, T. Agostinelli, P. G. Etchegoin, Y. Kim, T. D. Anthopoulos, P. N. Stavrinou, D. D. C. Bradley and J. Nelson, *Nat. Mater.*, 2008, **7**, 158.
18 Y. Yao, J. Hou, Z. Xu, G. Li and Y. Yang, *Adv. Funct. Mater.*, 2008, **18**, 1783.
19 Z. Xu, L.-M. Chen, G. Yang, C.-H. Huang, J. Hou, Y. Wu, G. Li, C.-S. Hsu and Y. Yang, *Adv. Funct. Mater.*, 2009, **19**, 1227.
20 D. S. Germack, C. K. Chan, B. H. Hamadani, L. J. Richter, D. A. Fischer, D. J. Gundlach and D. M. DeLongchamp, *Appl. Phys. Lett.*, 2009, **94**, 233303.
21 M.-S. Kim, B.-G. Kim and J. Kim, *ACS Appl. Mater. Interfaces*, 2009, **1**, 1264.
22 L. Zeng, C. W. Tang and S. H. Chen, *Appl. Phys. Lett.*, 2010, **97**, 053305.
23 S. Lee, S. Nam, H. Kim and Y. Kim, *Appl. Phys. Lett.*, 2010, **97**, 103503.
24 W. Ma, C. Yang, X. Gong, K. Lee and A. J. Heeger, *Adv. Funct. Mater.*, 2005, **16**, 1617.
25 G. Li, V. Shrotriya, J. Huang, Y. Yao, T. Moriarty, K. Emery and Y. Yang, *Nat. Mater.*, 2005, **4**, 864.
26 L.-M. Chen, Z. Hong, W. L. Kwan, C.-H. Lu, Y.-F. Lai, B. Lei, C.-P. Liu and Y. Yang, *ACS Nano*, 2010, **4**, 4744.
27 S. E. Shaheen, R. Radspinner, N. Peyghambarian and G. E. Jabbour, *Appl. Phys. Lett.*, 2001, **79**, 2996.
28 S. H. Park, A. Roy, S. Beaupre, S. Cho, N. Coates, J. S. Moon, D. Moses, M. Leclerc, K. Lee and A. J. Heeger, *Nat. Photonics*, 2009, **3**, 297.
29 H.-Y. Chen, J. Hou, S. Zhang, Y. Liang, G. Yang, Y. Yang, L. Yu, Y. Wu and G. Li, *Nat. Photonics*, 2009, **3**, 649.
30 V. Shrotriya, Y. Yao, G. Li and Y. Yang, *Appl. Phys. Lett.*, 2006, **89**, 063505.
31 M. A. Lampert and P. Mark, in *Current Injection in Solids*, Academic, New York, 1970.
32 A. Kumar, H.-H. Liao and Y. Yang, *Org. Electron.*, 2009, **10**, 1615.
33 J. Y. Kim, S. Noh, Y. M. Nam, J. Y. Kim, J. Roh, M. Park, J. J. Amsden, D. Y. Yoon, C. Lee and W. H. Jo, *ACS Appl. Mater. Interfaces*, 2011, **3**, 4279.
34 C.-J. Ko, Y.-K. Lin, F.-C. Chen and C.-W. Chu, *Appl. Phys. Lett.*, 2007, **90**, 063509.
35 V. D. Mihailetchi, J. Wildeman and P. W. M. Blom, *Phys. Rev. Lett.*, 2005, **94**, 126602.
36 S. Bange, M. Schubert and D. Neher, *Phys. Rev. B: Condens. Matter Mater. Phys.*, 2010, **81**, 035209.
37 J. Lorrmann, B. H. Badada, O. Inganäs, V. Dyakonov and C. Deibel, *J. Appl. Phys.*, 2010, **108**, 113705.
38 A. J. Mozer, N. S. Sariciftci, L. Lutsen, D. Vanderzande, R. Österbacka, M. Westerling and G. Juška, *Appl. Phys. Lett.*, 2005, **86**, 112104.
39 J. Nelson, *Phys. Rev. B: Condens. Matter*, 2003, **67**, 155209.
40 I. Montanari, A. F. Nogueira, J. Nelson, J. R. Durrant, C. Winder, M. A. Loi, N. S. Sariciftci and C. Brabec, *Appl. Phys. Lett.*, 2002, **81**, 3001.
41 A. Baumann, J. Lorrmann, D. Rauh, C. Deibel and V. Dyakonov, *Adv. Mater.*, 2012, **24**, 4381.
42 A. L. Fahrenbruch and J. Aranovich, in *Solar Energy Conversions Solid-State Physics Aspects*, Springer-Verlag, Berlin, Heidelberg, New York, 1979, vol. 31.
43 A. L. Fahrenbruch and H. R. Bube, in *Fundamentals of Solar Cells*, Academic, New York, 1981, p. 163.
44 C. Waldauf, M. C. Scharber, P. Schilinsky, J. A. Hauch and C. J. Brabec, *J. Appl. Phys.*, 2006, **99**, 104503.
45 J. H. Lee, S. Cho, A. Roy, H.-T. Jung and A. J. Heeger, *Appl. Phys. Lett.*, 2010, **96**, 163303.
46 L. J. A. Koster, E. C. P. Smits, V. D. Mihailetchi and P. W. M. Blom, *Phys. Rev. B: Condens. Matter Mater. Phys.*, 2005, **72**, 085205.
47 D. W. Sievers, V. Shrotriya and Y. Yang, *J. Appl. Phys.*, 2006, **100**, 114509.
48 A. Wagenpfahl, C. Deibel and V. Dyakonov, *IEEE J. Sel. Top. Quantum Electron.*, 2010, **16**, 1759.
49 G. F. Burkhard, E. T. Hoke and M. D. McGehee, *Adv. Mater.*, 2010, **22**, 3293.
50 C. Pina-Hernandez, J.-S. Kim, L. J. Guo and P.-F. Fu, *Adv. Mater.*, 2007, **19**, 1222.
51 V. Shrotriya, G. Li, Y. Yao, T. Morarty, K. Emery and Y. Yang, *Adv. Funct. Mater.*, 2006, **16**, 2016.

